minerals

MDPI

Article

Mechanism and Kinetics of the Reduction of Hematite to Magnetite with CO–CO_2 in a Micro-Fluidized Bed

Jianwen Yu, Yuexin Han *, Yanjun Li, Peng Gao and Wenbo Li

College of Resources and Civil Engineering, Northeastern University, Shenyang 110819, China; happy_yujianwen@163.com (J.Y.); liyanjun@mail.neu.edu.cn (Y.L.); gaopeng@mail.neu.edu.cn (P.G.); liwenbo@mail.neu.edu.cn (W.L.)

* Correspondence: dongdafulong@mail.neu.edu.cn.; Tel.: +86-024-8368-0162

Received: 28 August 2017; Accepted: 31 October 2017; Published: 1 November 2017

Abstract: The mechanism and kinetics of the reduction of hematite to magnetite in a laboratory-scale, micro-fluidized bed reactor were isothermally investigated. The procedure consisted of the isothermal heating in a flow of a 20%CO–80%CO_2 mixture at temperatures from 500 °C to 600 °C. It was found that the Avrami–Erofe'ev model of nucleation and 1D growth (n = 1.58) successfully described the phase transition of hematite to magnetite, and the value of activation energy ΔE_a of the reaction was estimated to be 48.70 kJ/mol. The microstructure properties for specimens with different conversion degrees were analyzed using the Brunauer, Emmett and Teller (BET) method and scanning electron microscopy (SEM). The results showed that the magnetite nuclei were needle-like, and the hematite specimens became thoroughly porous after complete reduction to magnetite. The physical and chemical processes of the reaction were also discussed.

Keywords: reduction kinetics; fluidized magnetization roasting; hematite; magnetite

1. Introduction

The preparation of magnetite (Fe_3O_4) has become of long-standing interest because of the diversified applications of magnetite in the industry as a pigment, in magnetic tapes, or as raw material for iron-making [1–3]. Therefore, it is of great interest to study innovative synthetic methods to reduce the production costs of magnetite and improve its production efficiency. Several chemical methods have been proposed to synthesize magnetite [4–8]. Fluidized reduction roasting has been proven to bean industrially economical and efficient method for the chemical synthesis of magnetite, with hematite as the raw material [9,10]. The reaction in fluidized bed reactors offers the advantages of a uniform temperature in the reactor, and of fast heat and mass transfer [11].

Several researchers have examined the reduction of synthetic Fe_2O_3 reagents or of hematite to magnetite by gaseous reductants, and the data reported can be summarized in Table 1. According to the reported results, the ΔE_a (activation energy) for the reduction of synthetic Fe_2O_3 reagents or for hematite to magnetite varies from 33.28 kJ/mol to 139.2 kJ/mol, and there are four mechanism models for this reaction, including the random nucleation model, the phase boundary model, the non-topochemical model, and the unimolecular model. The difference between these mechanism models may be caused by the different experimental conditions, which include thereactor type, the reduction temperature, the gaseous atmosphere, and the particle size. Especially, the solid material used in the previous experiments consistedmostly of synthetic Fe_2O_3 reagents with the same chemical composition as natural hematite (Fe_2O_3). However, the physicochemical properties, such as the specific surface area, density, hardness, and granularity of the synthetic Fe_2O_3 reagents and of natural hematite

are different. Therefore, the kinetics parameters and mechanisms for the reduction of synthetic Fe_2O_3 to magnetite cannot fully explain the process and mechanism for the reduction of hematite to magnetite.

Table 1. Summary of the activation energy values and reduction mechanisms reported in the literature.

Source	Material	Method	ΔE_a (kJ/mol)	Mechanism	Ref.
Shimokawabe et al.	Fe_2O_3/5%CO-Ar	Non-Isothermal (25–700 °C)	33.28–74.00	Random nucleation	[12]
Tiernan et al.	Fe_2O_3/5%H_2-He	Non-isothermal (25–650 °C)	96.02–105.3	Phase boundary	[13]
Trushenski et al.	Hematite/10%CO-CO_2	Isothermal (750–800 °C)	69–100	Non-topochemical model	[14]
Piotrowski et al.	Hematite/5.7%CO + 4.3%H_2-N_2	Isothermal (700–900 °C)	58.13	Random nucleation	[15]
Lin et al.	Fe_2O_3/5%H_2-N_2	Non-Isothermal (25–900 °C)	89.13	Unimolecular model	[16]
Jozwiak et al.	Fe_2O_3/5%CO-Ar	Non-Isothermal (25–1000 °C)	70	Not determined	[17]
Hou et al.	Fe_2O_3/5%H_2-Ar	Isothermal (440–490 °C)	105.4	Not determined	[18]
Pineau et al.	Fe_2O_3/10%H_2-N_2	Isothermal (220–680 °C)	75.9–114.1	Not determined	[19]
Munteanu et al.	Fe_2O_3/10%H_2-Ar	Non-Isothermal (290–480 °C)	139.2	Not determined	[20]
Gaviria et al.	Fe_2O_3/5%H_2-Ar	Isothermal (260–360 °C)	94–102	Not determined	[21]
Chakraborty	Fe_2O_3/5%H_2-Ar	Isothermal (575 °C)	115.7	Not determined	[22]
Wimmers et al.	Fe_2O_3/67%H_2-Ar	Non-Isothermal (290–480 °C)	124	Not determined	[23]
Colombon et al.	Fe_2O_3/100%H_2	Isothermal (250–400 °C)	108.7	Not determined	[24]
Hou et al.	Fe_2O_3/5%CO-Ar	Isothermal (400~500 °C)	75.4	Not determined	[25]

In this work, in order to avoid the overreduction of the newly generated magnetite to wüstite (FeO), a mixture of 20% CO–80% CO_2 was used as a reducing reagent, which was thermodynamically in equilibrium with the magnetite. The kinetics of the reduction of hematite to magnetite in a fluidized bed reactor at temperatures between 500 °C and 600 °C (the temperature range is consistent with the industrial production temperature) was studied for the first time. Meanwhile, the microstructure changes after reduction roasting were analyzed by the Brunauer, Emmett and Teller (BET) method and scanning electron microscopy (SEM), and the physical and chemical processes of the reduction of hematite to magnetite with CO–CO_2 in a micro-fluidized bed were also discussed.

2. Materials and Methods

2.1. Materials

The material used in this study was a powdered natural hematite ore (containing 93.5 % Fe_2O_3 and 6.5% SiO_2, *w*/*w*). The X-ray diffraction pattern of the hematite powder is presented in Figure 1, indicating that the main phase structures of the sample werehematite (Fe_2O_3) and quartz (SiO_2). The grain size of the hematite ore was 74 μm–100 μm. The SEM image of the sample is shown in Figure 2, indicating that the surface of the sample wasrough. The BET surface area and porosity volume of the hematite ore were 0.669 m^2/g and 0.003 m^3/g, respectively. A gas mixture of 20% CO–80% $CO_2$with a purity of 99.9%was used as a reducing agent, and nitrogen (N_2) with a purity of 99.9% was used as a protective gas.

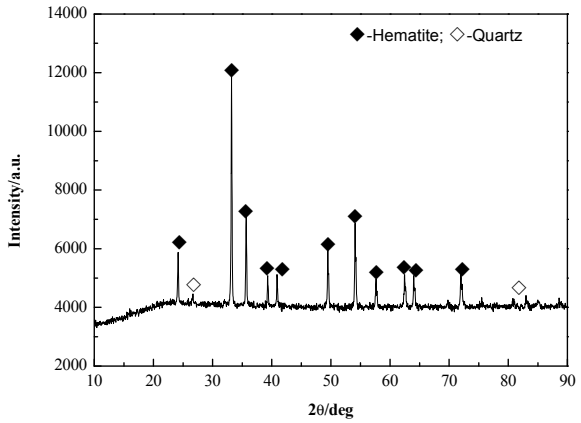

Figure 1. X-ray diffraction spectrogram of the pure hematite powder.

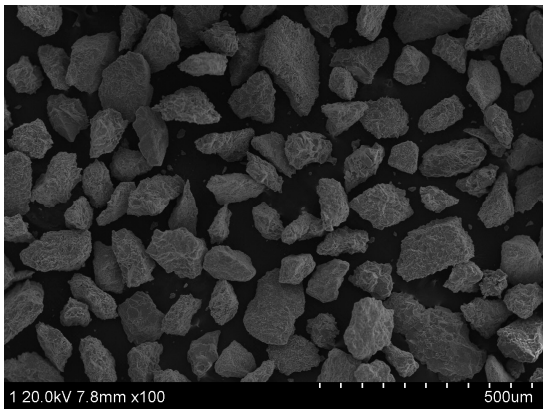

Figure 2. SEM image of the powdered hematite ore sample.

2.2. Experimental Apparatus and Procedures

All the experiments of this study were conducted in a cylindrical quartz fluidization furnace tube with an inner diameter of 20 mm, and the schematic diagram of the experimental apparatus is shown in Figure 3. A perforated quartz plate bed containing holes of 15 μm in diameter wasfitted in the middle of the fluidization furnace tube.

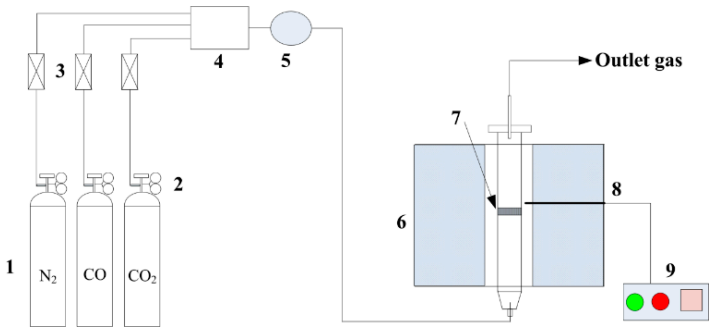

Figure 3. Schematic diagram of the experimental apparatus: 1, gas cylinder; 2, gas valve; 3, mass flow meter; 4, mixing cylinder; 5, gas drying; 6, heating furnace; 7, fluidized bed (porous quartz plate); 8, thermocouple; 9, temperature controller.

The powdered hematite ore was initially preheated (10 °C/min) under flowing nitrogen (1000 mL/min) to the predetermined temperature (selected from the 500 °C–600 °C range). At the defined

temperature, the nitrogen flow was switched to the flow of the reducing gas mixture (1000 mL/min, gas mixture composition: 20% CO + 80% CO_2). After roasting for a given time, the reducing gas mixture was switched back to pure nitrogen, and the reactor was cooled down to ambient temperature. Before entering the micro-fluidized bed reactor, gases were dried by anhydrous calcium chloride. All tests were carried out with 5 g of fresh hematite powder.

2.3. Methods

The surface area, porosity volume, and pore size measurements were carried out using the BET (liquid N_2) method based on the adsorption of N_2 at −197 °C, withan ASAP 2020-Physisorption Analyzer instrument (Micromeritics Instrument Corp, Atlanta, GA, USA), and the microstructures of the roasted specimens were analyzed by SEM (S-3400N; Hitachi, Ltd., Tokyo, Japan). The kinetics of the hematite–magnetite reduction process was determined by monitoring the change of ferrous oxide content (w_{FeO}) in the specimens during their transformation under selected isothermal conditions. At the end of the reduction test, the roasted specimens were ground to pass through a 74 μm sieve. The content of FeO (w_{FeO}) in the roasted specimens was determined by chemical analysis.

We considered the following chemical reaction for hematite to magnetite:

$$3Fe_2O_3 + CO \rightarrow 2Fe_3O_4 + CO_2 \quad (1)$$

It can be noted that, based on the above reaction's stoichiometry, the w_{FeO} of the roasted specimens corresponds to the conversion degree α (of Fe_2O_3 to Fe_3O_4). Based on the law of mass conservation, the numerical relationship between w_{FeO} and α is shown in Equation (2):

$$\alpha = 5w_{FeO}/(1.4 + 0.16w_{FeO}) \quad (2)$$

The reaction rate, r, can be calculated by the following Equation (3):

$$r = d_\alpha / d_t \quad (3)$$

3. Results and Discussion

3.1. Determination of the Kinetic Model

The $\alpha = f(t)$ and $r = f(t)$ experimental profiles, calculated with Equations (2) and (3), and corresponding to different process temperatures, are presented in Figures 4 and 5, respectively.

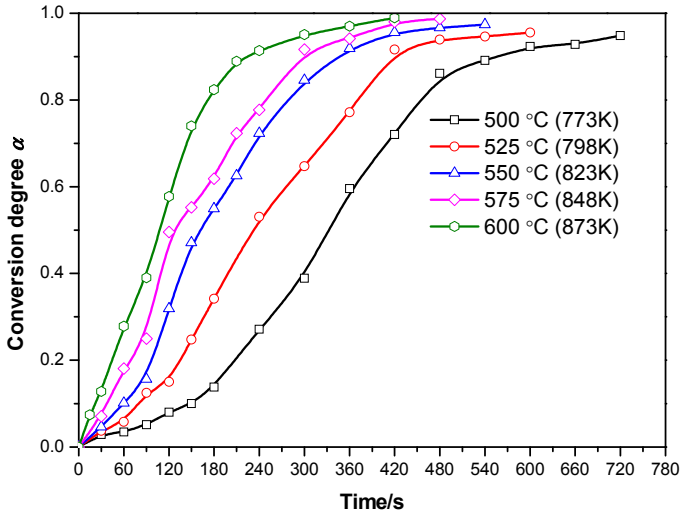

Figure 4. Conversion degree α vs. time for the selected process temperatures.

All $\alpha = f(t)$ conversion curves at different temperatures were S-shaped (Figure 4) and couldbe divided into three different periods, namely, induction, acceleration, and deceleration period (Figure 5). As shown in Figure 4, the incubation period shortened and the reaction rate increased with the increase of the roasting temperature.

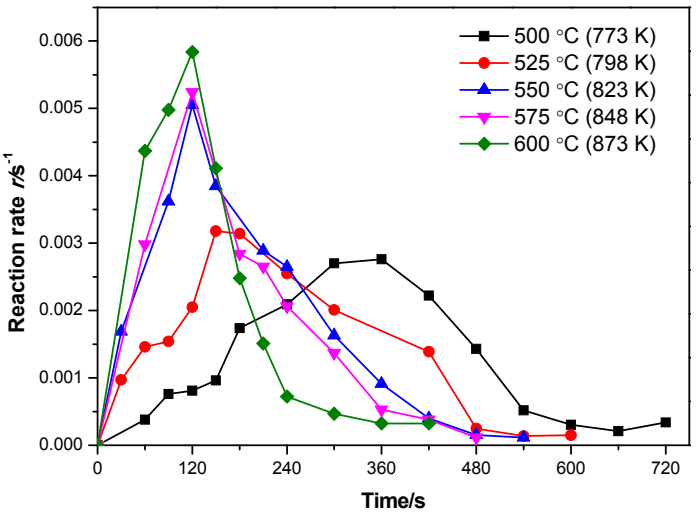

Figure 5. Reaction rate r vs. time for the selected process temperatures.

The S-shaped $\alpha = f(t)$ curves are commonly analyzed by the Hancock and Sharp's method [26,27]:

$$\alpha = 1 - \exp(-\beta t^n) \quad (4)$$

$$\ln(-\ln(1 - \alpha)) = \ln\beta + n\ln t \quad (5)$$

where α is the conversion degree of Fe_2O_3 to Fe_3O_4 at a certain time t, β is the isothermal crystallization rate constant, and n is the Avrami exponent related to the growth and morphology of the crystals.

The calculation results obtained by applying Equation (5) tothe test data are presented in Figure 6, and their linear fitting analysis resultsare listed in Table 2.

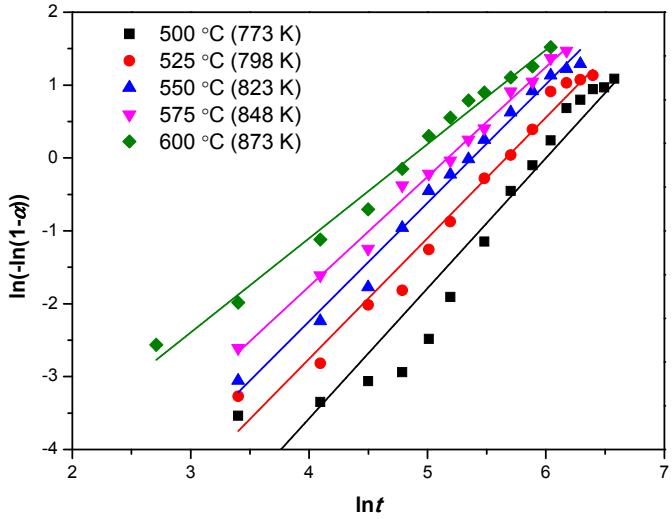

Figure 6. Linear fitting of the function $\ln(-\ln(1 - \alpha))$ vs. $\ln t$ for the selected process temperatures.

Table 2. Parameters of Equation (5) for the selected process temperatures.

No.	Temperature/°C	n	lnβ	Correlation Coefficient R
1	500 (773 K)	1.79	−10.71729	0.9642
2	525 (798 K)	1.66	−9.37611	0.9897
3	550 (823 K)	1.63	−8.74489	0.9944
4	575 (848 K)	1.51	−7.78061	0.9964
5	600 (873 K)	1.29	−6.26923	0.9948
Average		1.58	−8.57763	0.9879

An average value of n = 1.58 was obtained, suggesting that the universal Avrami–Erofe'ev kinetic model describing nucleation and growth processes, shown in Equation (6), mightbe applicable for the modeling of the Fe_2O_3 to Fe_3O_4 reductionreaction:

$$[-\ln(1-\alpha)]^{1/n} = kt \quad (6)$$

In this equation, the parameter k isthe kinetic (reaction rate) constant. Meanwhile, the values of n = 1−2 represent the 1D growth of nuclei [28]. Thus, this equationindicates that this phase transition of hematite to magnetite proceeded through a 1D growth process, suggesting that the newly generated magnetite nuclei wereneedle-like, which wasalso proven by Et-Tabirou, Swann, and Bahgat [29–31]. Additionally, the kinetic constant (k) values for different roasting temperatures could be obtained from the experimental $\alpha = f(t)$ data through the Avrami–Erofe'ev equation (n = 1.58). The calculation results obtained by applying Equation (6) to the test data are presented in Figure 7, and their linear fitting analysis results are listed in Table 3.

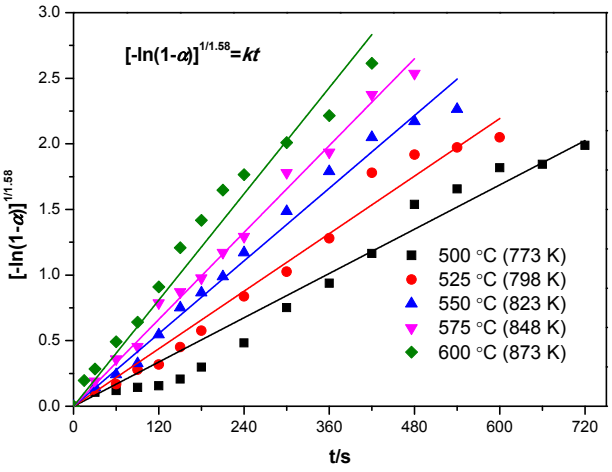

Figure 7. Linear fitting of the function $\ln[-\ln(1-\alpha)]^{1/1.58}$ vs. t for the selected process temperatures.

Table 3. Kinetic constant (k) values for the selected process temperatures studied.

No.	Temperature/°C	Kinetic Constant k/s^{-1}	Correlation Coefficient R
1	500 (773 K)	0.00281	0.9931
2	525 (798 K)	0.00365	0.9961
3	550 (823 K)	0.00462	0.9976
4	575 (848 K)	0.00552	0.9989
5	600 (873 K)	0.00675	0.9947

As shown in Table 3, the kinetic constant k increasedwith the increase of the roasting temperature, indicating that the required roasting time for the total conversion of Fe_2O_3 to $Fe_3O_4$was gradually shortened with the increase of the roasting temperature.

Figure 8 exhibits the graphical comparison between the experimental and the modeled values of $\alpha = f(t)$ using theAvrami–Erofe'ev topochemical kinetic model (n = 1.58). It is clearly visible that the experimental data do not exactly coincide with the theoretical predicted values. This is because this kinetic model only applies to the surface reaction of the hematite particles, without considering the influence of mass or heat transfer resistances during the reaction process [15]. However, the mass and heating transfer resistances occur, induced by the gradually thicker magnetite layer during the fluidized reduction process of hematite, and lead to a deviationbetween the experimental data and the theoretical predicted values.

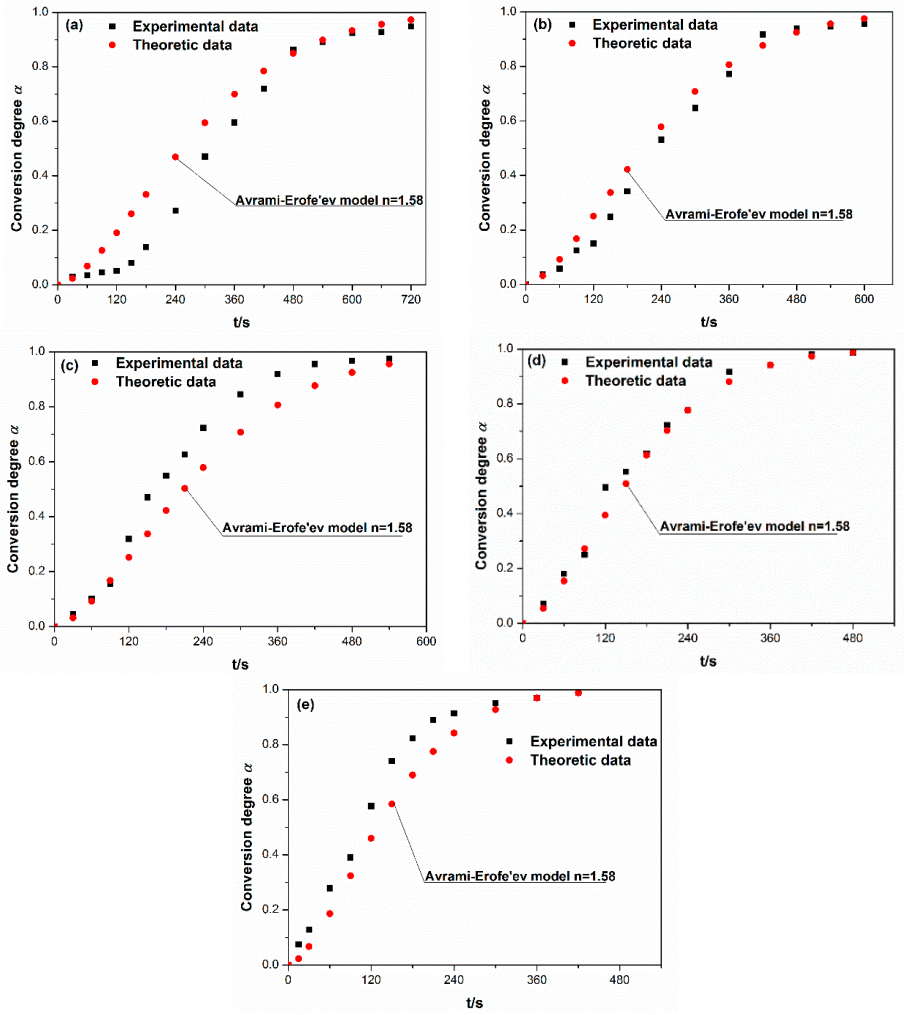

Figure 8. Comparison of the experimental data with the Avrami–Erofe'ev topochemical kinetic model (n = 1.58) applied in this study: (**a**) 500 °C; (**b**) 525 °C; (**c**) 550 °C; (**d**) 575 °C; (**e**) 600 °C.

The data from Table 3 were then usedto calculate the pre-exponential factor (A) and the activation energy (ΔE_a) values from the Arrhenius equations, Equations (7) and (8):

$$k = A \exp\left(-\frac{\Delta E_a}{RT}\right) \tag{7}$$

$$\ln k = \ln A - \frac{\Delta E_a}{R} \cdot \frac{1}{T} \tag{8}$$

where k is the kinetic constant, A the pre-exponential factor, R the gas constant (8.314 J/mol·K), and ΔE_a the activation energy. The linear fitting of the function ln$k$ vs. $1/T$ for the selected process temperatures

is plotted in Figure 9. From the regression calculations, the following were obtained: A = 5.58 s^{-1}, ΔE_a = 48.70 kJ/mol. Thus, $k = 5.58\exp(-48700/RT)$.

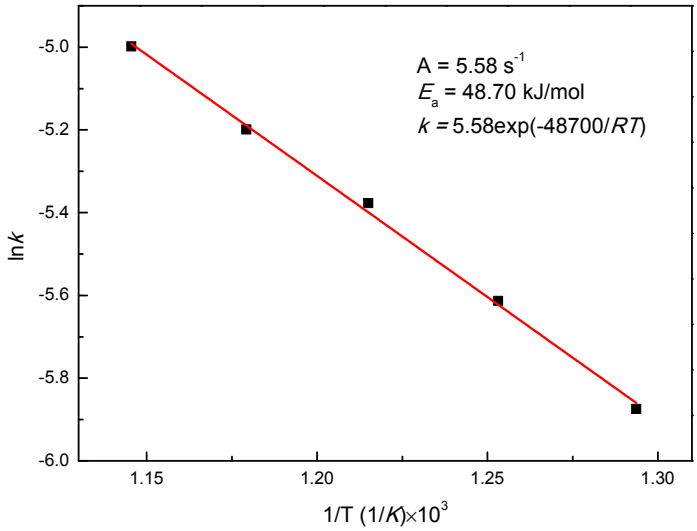

Figure 9. Arrhenius plot $\ln k = f(1/T)$ for the evaluation of the activation energy of the process.

3.2. Microstructure Changes after Reduction Roasting

In order to investigate the microstructure changes during the reduction process, measurements of the surface area, porosity volume, and pores size were carried out for specimens with different conversion degrees, using the BET (liquid N_2) method. The resultsareshown in Table 4. It is obvious that the surface area, porosity volume, and pore size of the specimens greatly increased with the increasing of the conversion degree of hematite to magnetite.

Table 4. Specific surface properties for specimens with different conversion degrees.

No.	Experimental Conditions	Conversion Degree α/%	BET Surface Area/$m^2 \cdot g^{-1}$	Porosity Volume/$cm^3 \cdot g^{-1}$	Pore Size/nm
1	Raw hematite	0	0.6693	0.002659	15.89
2	Reduction at 500 °C for 3 min	13.8	0.7803	0.005688	29.15
3	Reduction at 575 °C for 2.5 min	55.3	1.0831	0.010966	40.50
4	Reduction at 550 °C for 9 min	97.4	1.4751	0.020231	54.86

Figure 10 presents the microstructures of roasted samples at 600 °C atdifferent times. As shown in Figure 10a, the conversion of hematite to magnetite initially occurred at the outer surface of the hematite particles because of the presence of an external magnetite layer in the original hematite particle and of the fact that the fresh magnetite nuclei were needle-like (Figure 10d). With time, the needle-like magnetite nuclei increased, and the fresh magnetite particles were randomly filled with micropores and cracks (Figure 10b). Eventually, the original hematite particles were completely transformed into magnetite particles with a porous structure (Figure 10c). As mentioned above, the reduction process of hematite to magnetite may be theoretically divided into three periods, namely, an induction period ($0 < \alpha < 0.15$), an acceleratory period ($0.15 < \alpha < 0.50$), and a deceleratory period ($0.5 < \alpha < 1$) [15,28]. In the initial induction period, the fresh microcracks were formed as a result of normal swelling due to the crystal structure difference between the starting hematite (hexagonal closed-packed) and the newly

formed magnetite (cubic spinal). During the second acceleratory period, the microcracks increased and enlarged with more magnetite nuclei formation, and theirgrowth facilitated the gas diffusion to the unreacted inner hematite layers. Therefore, the reduction reaction progressed. As the conversion degree increased, the reduction entered the final deceleratory period, which was characterized by the termination of growth upon the impingement of different growth regions or their reaching the grain boundaries. As a result, the hematite specimens became wholly porous after the complete reduction to magnetite.

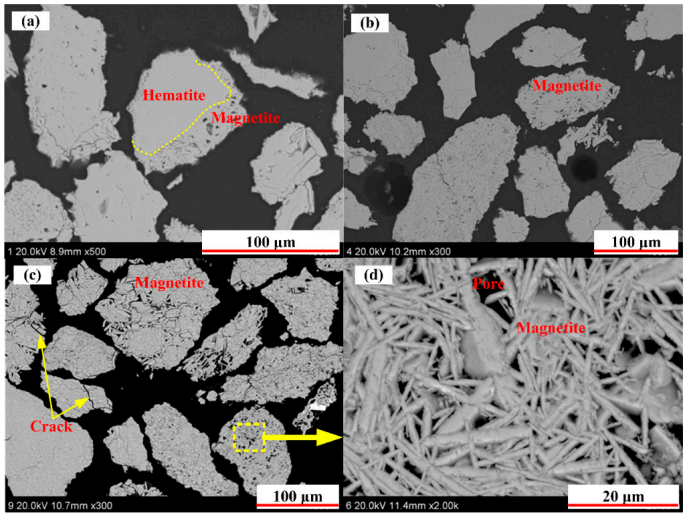

Figure 10. Microstructure of roasted samples atdifferent times at 600 °C: (**a**) 30 s (α = 10%); (**b**) 120 s (α = 50%); (**c**) and (**d**) 420 s (α = 100%).

3.3. Physical and Chemical Processes

Based on the above analysis, the physical and chemical processes duringthe reduction of hematite to magnetite in a micro-fluidized bed reactor are shown schematically in Figure 11.

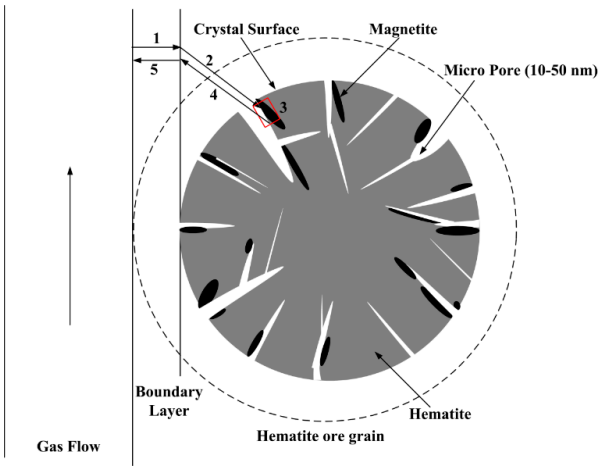

Figure 11. Physical and chemical processes around and inside the hematite ore grain in the micro-fluidized bed reactor: steps 1 and 5 represent thediffusion through the gas boundary layer situated around the hematite ore grain; steps 2 and 4 represent the gas diffusion through the pores of the hematite ore grain; step 3 represents the phase–interface reaction at the crystal surface, and the diffusion of the iron ions through the dense magnetite layers.

The hematite ore particles were fluidized in the reactor with the reducinggas mixture (1000 mL/min). The reducing gas CO diffused through the boundary layer, reaching the external surface of the hematite particles and continuing further into the micropores to the internal surface of the hematite grains. The phase–interface reaction described by Equation (1) occurred at this surface, where the reducing gas picked up oxygen and freed two electrons [9,11,29]:

$$CO + O^{2-} \rightarrow CO_2 + 2e^- \quad (9)$$

The electrons remained in the lattice where theyreduced Fe^{3+} to Fe^{2+}, as shown in Equation (10).

$$Fe^{3+} + e^- \rightarrow Fe^{2+} \quad (10)$$

The generated ferrous ions and the electrons diffused through the magnetite product layer into the hematite core, where the hematite lattice deformed, and additional magnetite was formed through lattice reconstruction [9,11,29]:

$$4Fe_2O_3 + Fe^{2+} + 2e^- \rightarrow 3Fe_3O_4 \quad (11)$$

Oxygen would diffuse from the hematite core to the external border of magnetite, but the mobility of the oxygen anions in the magnetite was negligible in comparison with the ferrous cations [11]. The gaseous reaction product CO_2 migrated back to the gas flow where it could be removed from the fluidized bed reactor [11]. As the above process proceeded, the reduction reaction progressively extended to the inner layer. Finally, the hematite particles were completely reduced to magnetite [9]. The actual reaction is illustrated in all its phasesin Figure 12, which is modified from [11].

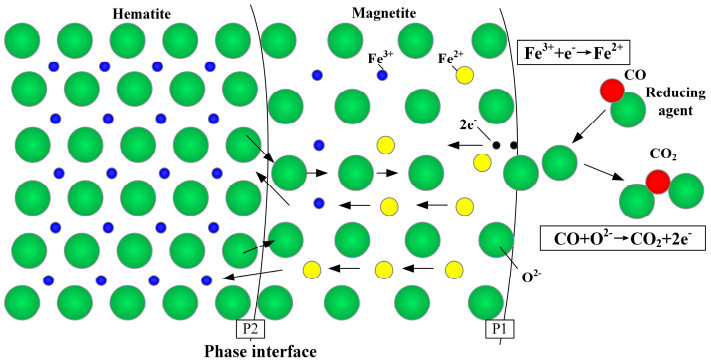

Figure 12. Atomic model for the reduction of hematite to magnetite by CO.

4. Conclusions

In this study, the kinetics of the reduction of hematite to magnetite with 20% CO–80% CO_2 in a micro-fluidized bed reactor was investigated for the first time. The reduction mechanism was also discussed. The following are the major findings obtained in this study:

(1) The Avrami–Erofe'ev model of nucleation and 1D growth (n = 1.58) was successfully applied to describe the phase transition of hematite to magnetite, and the value of activation energy ΔE_a of the reaction was estimated to be 48.70 kJ/mol.

(2) The newly formed magnetite nuclei were needle-like in shape. Microcracks were formed and increased asthe magnetite nuclei formed, and thus the original hematite sample became porous after complete reduction to magnetite.

(3) Micropores or cracks induced by normal swelling were conducive to the reduction of hematite to magnetite.

Acknowledgments: This work was funded by the National Science Foundation of China (Grant No. 51674064, 51674065, 51604064 and 51734005), and the Fundamental Research Funds for National University (Grant No. N140108001, N150103003 and N150106003).

Author Contributions: Jianwen Yu and Yuexin Han conceived and designed the experiments; Jianwen Yu and Yanjun Li performed the experiments; Peng Gao and Jianwen Yu analyzed the data; Yuexin Han and Yanjun Li contributed reagents/materials/analysis tools; Jianwen Yu, Wenbo Li, and Yuexin Han wrote the paper.

Conflicts of Interest: The authors declare no conflict of interest.

References

1. Yu, J.W.; Han, Y.X.; Li, Y.J.; Gao, P.; Sun, Y.S. Separation and recovery of iron from a low-grade carbonate-bearing iron ore using magnetizing roasting followed by magnetic separation. *Sep. Sci. Technol.* **2017**, *52*, 1768–1774. [CrossRef]
2. Legodi, M.A.; Waal, D.D. The preparation of magnetite, goethite, hematite and maghemite of pigment quality from mill scale iron waste. *Dyes Pigments* **2007**, *74*, 161–168. [CrossRef]
3. Wan, S.; Huang, J.; Yan, H.; Liu, K. Size-controlled preparation of magnetite nanoparticles in the presence of graft copolymers. *J. Mater. Chem.* **2006**, *16*, 298–303. [CrossRef]
4. Xu, J.; Yang, H.; Fu, W.; Du, K.; Sui, Y.; Chen, J.; Zeng, Y.; Li, M.; Zou, G. Preparation and magnetic properties of magnetite nanoparticles by sol-gel method. *J. Magn. Magn. Mater.* **2007**, *309*, 307–311. [CrossRef]
5. Chen, S.; Feng, J.; Guo, X.; Hong, J.; Ding, W. One-step wet chemistry for preparation of magnetite nanorods. *Mater. Lett.* **2005**, *59*, 985–988. [CrossRef]
6. Rabelo, D.; Lima, E.C.D.; Reis, A.C.; Nunes, W.C.; Novak, M.A.; Garg, V.K.; Oliveira, A.C.; Morais, P.C. Preparation of magnetite nanoparticles in mesoporous copolymer template. *Nano Lett.* **2001**, *1*, 105–108. [CrossRef]
7. Lee, H.S.; Lee, W.C.; Furubayashi, T. A comparison of coprecipitation with microemulsion methods in the preparation of magnetite. *J. Appl. Phys.* **1999**, *85*, 5231–5233. [CrossRef]
8. Hu, F.; Li, Z.; Tu, C.; Gao, M. Preparation of magnetite nanocrystals with surface reactive moieties by one-pot reaction. *J. Colloid Interface Sci.* **2007**, *311*, 469–474. [CrossRef] [PubMed]
9. Yu, Y.; Qi, C. Magnetizing roasting mechanism and effective ore dressing process for oolitic hematite ore. *J. Wuhan Univ. Technol. Mater. Sci. Ed.* **2011**, *26*, 176–181. [CrossRef]
10. Li, Y.J.; Wang, R.; Han, Y.X.; Wei, X.C. Phase transformation in suspension roasting of oolitic hematite ore. *J. Cent. South Univ.* **2015**, *22*, 4560–4565. [CrossRef]
11. Feilmayr, C.; Thurnhofer, A.; Winter, F.; Mali, H.; Schenk, J. Reduction behavior of hematite to magnetite under fluidized bed conditions. *ISIJ Int.* **2004**, *44*, 1125–1133. [CrossRef]
12. Shimokawabe, M.; Furuichi, R.; Ishii, T. Influence of the preparation history of α-Fe_2O_3 on its reactivity for hydrogen reduction. *Thermochim. Acta* **1979**, *28*, 287–305. [CrossRef]
13. Tiernan, M.J.; Barnes, P.A.; Parkes, G.M. Reduction of iron oxide catalysts: The investigation of kinetic parameters using rate perturbation and linear heating thermoanalytical techniques. *J. Phys. Chem. B* **2001**, *105*, 220–228. [CrossRef]
14. Trushenski, S.P.; Li, K.; Philbrook, W.O. Non-topochemical reduction of iron oxides. *Metall. Trans.* **1974**, *5*, 1149–1158. [CrossRef]
15. Piotrowski, K.; Mondal, K.; Wiltowski, T.; Dydo, P.; Rizeg, G. Topochemical approach of kinetics of the reduction of hematite to wüstite. *Chem. Eng. J.* **2007**, *131*, 73–82. [CrossRef]
16. Lin, H.Y.; Chen, Y.W.; Li, C. The mechanism of reduction of iron oxide by hydrogen. *Thermochim. Acta* **2003**, *400*, 61–67. [CrossRef]
17. Jozwiak, W.K.; Kaczmarek, E.; Maniecki, T.P.; Ignaczak, W.; Maniukiewicz, W. Reduction behavior of iron oxides in hydrogen and carbon monoxide atmospheres. *Appl. Catal. A Gen.* **2007**, *326*, 17–27. [CrossRef]
18. Hou, B.L.; Zhang, H.Y.; Li, H.Z.; Zhu, Q.S. Study on kinetics of iron oxide reduction by hydrogen. *Chin. J. Chem. Eng.* **2012**, *20*, 10–17. [CrossRef]
19. Pineau, A.; Kanari, N.; Gaballah, I. Kinetics of reduction of iron oxides by H_2: Part I: Low temperature reduction of hematite. *Thermochim. Acta* **2006**, *447*, 89–100. [CrossRef]
20. Munteanu, G.; Ilieva, L.; Andreeva, D. Kinetic parameters obtained from TPR data for α-Fe_2O_3 and Auα-Fe_2O_3 systems. *Thermochim. Acta* **1997**, *291*, 171–177. [CrossRef]

21. Gaviria, J.P.; Bohe, A.; Pasquevich, A.; Pasquevich, D.M. Hematite to magnetite reduction monitored by Mössbauer spectroscopy and X-ray diffraction. *Phys. B Condens. Matter* **2007**, *389*, 198–201. [CrossRef]
22. Chakraborty, A. Kinetics of the reduction of hematite to magnetite near its Curie transition. *J. Magn. Magn. Mater.* **1999**, *204*, 57–60. [CrossRef]
23. Wimmers, O.J.; Arnoldy, P.; Moulijn, J.A. Determination of the reduction mechanism by temperature-programmed reduction: Application to small iron oxide (Fe_2O_3) particles. *J. Phys. Chem.* **1986**, *90*, 1331–1337. [CrossRef]
24. Colombo, U.; Gazzarrini, F.; Lanzavecchia, G. Mechanisms of iron oxides reduction at temperatures below 400 °C. *Mater. Sci. Eng.* **1967**, *2*, 125–135. [CrossRef]
25. Hou, B.; Zhang, H.; Li, H.; Zhu, Q. Determination of the intrinsic kinetics of iron oxide reduced by carbon monoxide in an isothermal differential micro-packed bed. *Chin. J. Chem. Eng.* **2015**, *23*, 974–980. [CrossRef]
26. Paik, Y.; Osegovic, J.P.; Wang, F.; Bowden, W.; Grey, C.P. ^{2}H MAS NMR studies of the manganese dioxide tunnel structures and hydroxides used as cathode materials in primary batteries. *J. Am. Chem. Soc.* **2001**, *123*, 9367–9377. [CrossRef] [PubMed]
27. Wang, H.; Thomson, W.J. Binary kinetics in the Y-Ba-Cu system: 2. Nanosized particles. *AIChE J.* **1995**, *41*, 1790–1797. [CrossRef]
28. Liu, H.; Sullivan, R.M.; Hanson, J.C.; Grey, C.P.; Martin, J.D. Kinetics and mechanism of the β- to α-$CuAlCl_4$ phase transition: A time-resolved ^{63}Cu MAS NMR and powder X-ray diffraction study. *J. Am. Chem. Soc.* **2001**, *123*, 7564–7573. [CrossRef] [PubMed]
29. Et-Tabirou, M.; Dupre, B.; Gleitzer, C. Hematite single crystal reduction into magnetite with CO-CO_2. *Metall. Trans. B* **1988**, *19*, 311–317. [CrossRef]
30. Swann, P.R.; Tighe, N.J. High voltage microscopy of the reduction of hematite to magnetite. *Metall. Trans. B* **1977**, *8*, 479–487. [CrossRef]
31. Bahgat, M. Magnetite surface morphology during hematite reduction with CO/CO_2 at 1073 K. *Mater. Lett.* **2007**, *61*, 339–342. [CrossRef]